Journal of Physics: Conference Series **384** (2012) 012014 doi:10.1088/1742-6596/384/1/012014

Light Higgs and neutralino dark matter in the NMSSM

Daniel E. Lopez-Fogliani

Laboratoire de Physique Théorique, Université Paris-Sud, F-91405 Orsay, France

Abstract.

The next-to-minimal supersymmetric standard model (NMSSM) is a R-parity conserving model that solves the μ-problem of the minimal supersymmetric standard model (MSSM) by adding a singlet superfield. Here we study different aspects of this model. Firstly, using Bayesian statistics, we discuss the constrained next-to-minimal supersymmetric standard model (CNMSSM) scenario. We place special emphasis on analysing the neutralino as a dark matter candidate. Additionally, using the nested sampling (NS) algorithm, we focus our analysis on a particular region of the parameter space. Results obtained scanning the low energy parameter space of the NMSSM, searching for low mass neutralinos, are discussed.

1. Introduction

In the next-to-minimal supersymmetric standard model (NMSSM) the singlet field mixes with the minimal supersymmetric standard model (MSSM) Higgses, and the singlino field mixes with the MSSM neutralinos, offering a richer phenomenology. In the general case, it is possible to have light neutralinos, and in addition it is also possible to have a very light Higgs, which is experimentally viable for a sufficiently high singlet composition [1]. In particular, the exchange of very light Higgses can lead to large direct detection cross sections, within the reach of the present generation of dark matter detectors [2, 3].
The NMSSM superpotential is,

$$W = \epsilon_{ij}\left(Y_u\, H_2^j\, Q^i\, u + Y_d\, H_1^i\, Q^j\, d + Y_e\, H_1^i\, L^j\, e\right) - \epsilon_{ij}\lambda\, S\, H_1^i H_2^j + \frac{1}{3}\kappa S^3\,. \qquad (1)$$

In the context of supergravity, SUGRA, the soft breaking terms are giving by:

$$\begin{aligned}-\mathcal{L}_{\rm soft} =& m^2_{\tilde{Q}}\,\tilde{Q}^*\,\tilde{Q} + m^2_{\tilde{U}}\,\tilde{u}^*\,\tilde{u} + m^2_{\tilde{D}}\,\tilde{d}^*\,\tilde{d} + m^2_{\tilde{L}}\,\tilde{L}^*\,\tilde{L} + m^2_{\tilde{E}}\,\tilde{e}^*\,\tilde{e} \\ &+ m^2_{H_d}\,H^*_d\,H_d + m^2_{H_u}\,H^*_u H_u + m^2_S\,S^*S \\ &+ \epsilon_{ij}\,\Big(A_u\,Y_u\,H^j_u\,\tilde{Q}^i\,\tilde{u} + A_d\,Y_d\,H^i_d\,\tilde{Q}^j\,\tilde{d} + A_e\,Y_e\,H^i_d\,\tilde{L}^j\,\tilde{e} + \text{H.c.}\Big) \\ &+ \left(-\epsilon_{ij}\lambda\,A_\lambda S H^i_d H^j_u + \frac{1}{3}\kappa\,A_\kappa\,S^3 + \text{H.c.}\right) \\ &- \frac{1}{2}\,\left(M_3\,\lambda_3\,\lambda_3 + M_2\,\lambda_2\,\lambda_2 + M_1\,\lambda_1\,\lambda_1 + \text{H.c.}\right)\,. \end{aligned} \tag{2}$$

In addition to terms from $\mathcal{L}_{\rm soft}$, the tree-level scalar Higgs potential receives the usual D and F term contributions:

$$\begin{aligned} V_D =& \frac{g_1^2+g_2^2}{8}\left(|H_d|^2 - |H_u|^2\right)^2 + \frac{g_2^2}{2}|H_d^\dagger H_u|^2\,, \\ V_F =& |\lambda|^2\left(|H_d|^2|S|^2 + |H_u|^2|S|^2 + |\epsilon_{ij}H^i_d H^j_u|^2\right) + |\kappa|^2|S|^4 \\ &- \left(\epsilon_{ij}\lambda\kappa^* H^i_d H^j_u S^{*2} + \text{H.c.}\right)\,. \end{aligned} \tag{3}$$

When the scalar component of S acquires a VEV, an effective interaction $\mu H_1 H_2$ is generated, with $\mu \equiv \lambda\langle S\rangle$. We refer to [2] for a detailled analysis of the Higgs scalar potential and minimization conditions.

Using the minimization equations we can re-express the soft breaking Higgs masses in terms of λ, κ, A_λ, A_κ, $v_d = \langle H^0_d\rangle$, $v_u = \langle H^0_u\rangle$ (with $\tan\beta = v_u/v_d$), and $s =< S >$:

$$m^2_{H_d} = -\lambda^2\left(s^2 + v^2\sin^2\beta\right) - \frac{1}{2}M_Z^2\cos 2\beta + \lambda s\tan\beta\left(\kappa s + A_\lambda\right)\,, \tag{4}$$

$$m^2_{H_u} = -\lambda^2\left(s^2 + v^2\cos^2\beta\right) + \frac{1}{2}M_Z^2\cos 2\beta + \lambda s\cot\beta\left(\kappa s + A_\lambda\right)\,, \tag{5}$$

$$m^2_S = -\lambda^2 v^2 - 2\kappa^2 s^2 + \lambda\kappa v^2\sin 2\beta + \frac{\lambda A_\lambda v^2}{2s}\sin 2\beta - \kappa A_\kappa s\,, \tag{6}$$

In the next sections, to conduct the investigation of the parameter space of the model we use the nested sampling (NS) algorithm [4], implemented in the Bayesian interface tool `Multinest` [5], that is incorporated into the `SuperBayeS` [6] and NMSPEC [7] packages. Details of the analysis are given in the following next sections.

In section 2 we are going to discuss the results obtained in [8], regarding the investigation of the constrained NMSSM, CNMSSM, using Bayesian statistics.

The NS algorithm is very powerful, allowing us to scan over the parameter space of the NMSSM. Particular regions of the parameter space can be studied using this technique. As for example, the analysis of the ideal Higgs scenario carried out in [9]. Nevertheless to say, statistical interpretation must be taken with great care when particular regions of the parameter space are scanned. However the power of this technique can help to have a better

CNMSSM parameters θ	SM (nuisance) parameters ψ
$50 < m_{1/2} < 4$ TeV	$160 < M_t < 190$ GeV
$50 < m_0 < 4$ TeV	$4 < m_b(m_b)^{\overline{MS}} < 5$ GeV
$\lvert A_0 \rvert < 7$ TeV	$0.10 < \alpha_s(M_Z)^{\overline{MS}} < 0.13$
$2 < \tan\beta < 65$	
$10^{-3} < \lambda < 0.7$	

Table 1. Initial ranges for our basis parameters $m = (\theta, \psi)$.

understanding of a particular chosen region of the parameter space of the model. For an analysis of the ideal Higgs scenario using this scan technique we refer the interested reader to [9].

In section 3, based in a scan of the low mass parameters space using the power of the NS algorithm, we focus our investigation in the low mass neutralinos region [10].

2. The CNMSSM under the light of a Bayesian analysis

In this section we want to discuss a satistical Bayesian analysis of the CNMSSM. In this case the boundary conditions at the grand unification scale $M_{\rm GUT} \simeq 2 \times 10^{16}$ GeV are analogous to those of the CMSSM, with the exception of m_S. We took m_S indenpendent from m_0, and κ, m_S and s are fixed by the minimization equations (4)-(6) which leads to five continuous free parameters of the CNMSSM: $m_{1/2}$, m_0, A_0, $\tan\beta$ and λ. In addition we fix sgn(μ), chosen $\lambda > 0$ (without loss of generality [2]) and $s > 0$.

We adopt flat prior in $\log m_{1/2}$, $\log m_0$, A_0, $\tan\beta$ and λ, with the last two quantities taken at the scale $M_{\rm SUSY}$. In Table 1 we give the range where our priors vary.

For the nuisance parameters flat priors (although this is not important as they are directly constrained by measurements) are used as well as Gaussian likelihoods representing the experimental observations (see [8] for details).

Mass spectra and observables quantities are computed as was explained in [8], using NMSPEC Ref. [7]. The scanning technique adopted is a "nested sampling" (NS) method [4] as implemented in the MultiNest [11] algorithm, which computes the Bayesian evidence primarily but produces posterior pdfs in the process. MultiNest provides an extremely efficient sampler even for likelihood functions defined over a parameter space of large dimensionality with a very complex structure. (See, *e.g.*, Refs. [12, 13].) We list the observables that were included in the likelihood function in Table 2, for details see [8].

To start the discussion of the results, we show Fig. 1. Focusing on the left panel in the plane spanned by $m_{1/2}$ and m_0, we can see some prominent features: a rather strong preference for the stau coannihilation region of $m_{1/2} \gtrsim m_0 \lesssim 0.5$ TeV, although the 68% total probability region extends to larger m_0 because of the pseudoscalar funnel effect contribution

Observable	Mean value	Uncertainties		Ref.
	η	σ (exper.)	τ (theor.)	
$\delta(g-2)_\mu \times 10^{10}$	29.5	8.8	1	[14]
$BR(\overline{B} \to X_s\gamma) \times 10^4$	3.55	0.26	0.21	[14]
$BR(\overline{B}_u \to \tau\nu) \times 10^4$	1.32	0.49	0.38	[15]
$\Omega_\chi h^2$	0.1099	0.0062	$0.1\,\Omega_\chi h^2$	[16]
	Limit (95% CL)		τ (theor.)	Ref.
$BR(\overline{B}_s \to \mu^+\mu^-)$	$< 5.8 \times 10^{-8}$		14%	[17]
m_h	As implemented in NMSSMTools.			[7]
sparticle masses	As implemented in NMSSMTools.			[7]

Table 2. Summary of the observables used in the analysis. Upper part: Observables for which a positive measurement has been made. $\delta(g-2)_\mu$ denotes the discrepancy between the experimental value and the SM prediction of the anomalous magnetic moment of the muon $(g-2)_\mu$. For central values of the SM input parameters used here, the SM value of $BR(\overline{B} \to X_s\gamma)$ is 3.11×10^{-4}, while the theoretical error of 0.21×10^{-4} includes uncertainties other than the parametric dependence on the SM nuisance parameters, especially on M_t and $\alpha_s(M_Z)^{\overline{MS}}$. For each quantity we use a likelihood function with mean η and standard deviation $s = \sqrt{\sigma^2 + \tau^2}$, where σ is the experimental uncertainty and τ represents our estimate of the theoretical uncertainty (see Ref. [18] for details). Lower part: Observables for which only limits currently exist. The likelihood function is given in Ref. [18], including in particular a smearing out of experimental errors and limits to include an appropriate theoretical uncertainty in the observables in $BR(\overline{B}_s \to \mu^+\mu^-)$. The limit on the light Higgs mass m_h is applied in a simplified way, see text for details.

to $\Omega_\chi h^2$. The wedge of $m_{1/2} \gg m_0$ is disallowed because of charged LSP (normally the stau). On the right panel we can see that big and low values of $\tan\beta$ are preferred.

On the left panel of Fig. 2 we can see that in general λ prefers to be small, which leads to a statistical preference for a very CMSSM-like behavior. Large values of λ, bigger than around 0.6 are disfavored due to a Landau pole in the running of the parameter. At "intermediate" values, $0.1 \lesssim \lambda \lesssim 0.6$, the constraints become weaker but there remain problems with tachyons, seen most clearly in the (λ, κ) plane, presented in Fig. 2, which also shows how both parameters are rather closely correlated, $\kappa \propto \lambda$, and favor small values, towards the decoupling limit. The region with $\kappa \gg \lambda$ is disfavored by the presence of tachyonic CP-odd scalars, and similarly with CP-even scalars for $\kappa \ll \lambda$. The preference for low λ could be due to the fact that there are fewer tachyonic directions in the potential close to the decoupling limit $\lambda \to 0$ (for this to happen $\lambda \lesssim 0.1$ is sufficient). For a more detailed discussion, see Ref. [2].

On the right panel of Fig. 2 we present the 2D posterior pdfs in the usual plane spanned by

the spin-independent cross section σ_p^{SI} and the neutralino mass m_χ. For comparison, some of the most stringent 90% CL experimental upper limits are also marked [19, 20, 21, 22, 23, 24], although they have not been imposed in the likelihood because of substantial astrophysical uncertainties, especially in the value of the local density.

Several key features can be seen on the right panel of Fig. 2. The banana shaped high-probability region corresponds to the Higgs funnel and the stau coannihilation regions. The horizontal branch of $\sigma_p^{SI} \simeq 7 \times 10^{-8}$ pb corresponds to the focus point region of large m_0. Next, the overall shape rather closely resembles the case of the CMSSM, see, *e.g.*, Fig. 18 of Ref. [12] or Fig. 13 of Ref. [18].

Basically the whole 68% and 95% total probability regions are likely to be within the planned reach of 10^{-10} pb of future 1-tonne detectors. Some of the currently operating detectors are already probing some of the high probability regions, and with a "modest" improvement down to $\sim 10^{-8}$ pb, they will be testing some of the most likely cross sections.

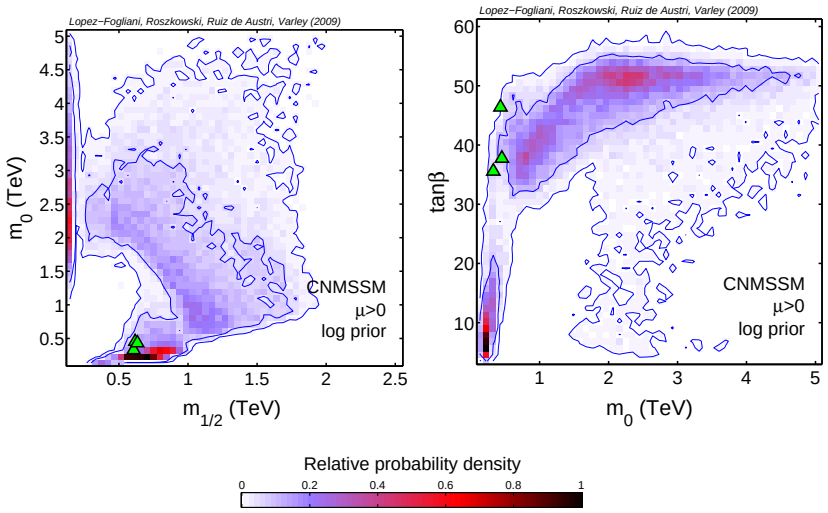

Figure 1. The 2D relative probability density functions in the planes spanned by the CNMSSM parameters $m_{1/2}$, m_0, $\tan\beta$ and A_0. The pdfs are normalized to unity at their peak. The inner (outer) blue solid contours delimit regions encompassing 68% and 95% of the total probability, respectively. All other basis parameters, both CNMSSM and SM ones, in each plane have been marginalized over (i.e., integrated out). Green triangles indicate some of the best fit points.

3. Low mass neutralinos

In this section we are going to use the power of the NS algorithm to analyse a particular region of the parameter space, searching for low mass neutralinos. Statistical interpretations in this case must be taken with great care.

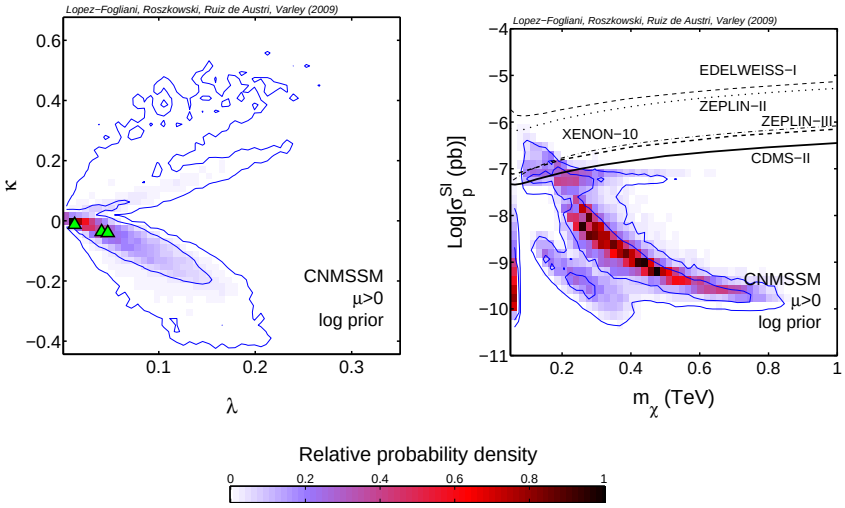

Figure 2. Left: The 2D relative pdfs in the plane of (λ, κ). Right: For the dark matter spin-independent cross section σ_p^{SI} vs the neutralino mass m_χ we show the 2D relative probability density.

Instead of scan the parameters of the model at the GUT scale, as in the previous section, we are going to make a scan of the parameters at low scale.

We are going to assume minimal flavour violation, and perform a scan as described in [10], over the following NMSSM parameters:

$$M_1, M_2, \mu, m_A, m_{\tilde{l}_L}, m_{\tilde{l}_R}, A_\kappa, \tilde{A}, \tan\beta, \lambda, \kappa. \tag{7}$$

where m_A denotes the CP-odd Higgs that is mainly doublet-like, as defined in the NMSPEC code [7]. For simplicity, we take all the trilinear couplings degenerated at EW scale: $A_t = A_b = A_\tau = \tilde{A}$, with the exception of A_κ, which freedom is going to be crucial in order to find low mass neutralinos. We take all left-handed slepton soft mass parameters to be family degenerate (i.e., $m_{\tilde{e}_L} = m_{\tilde{\mu}_L} = m_{\tilde{\tau}_L} = m_{\tilde{l}_L}$), and likewise for their right-handed partners. On the other hand, gluino and squark masses will not play any significant role in determining either the relic density $\Omega_\chi h^2$ or the spin-independent elastic scattering cross section σ_p^{SI}, and hence we fix them at 1 TeV. In order to focus our scan towards the low mass region of a few GeV, we adopt a log prior distribution of the bino mass M_1, which primarily determines the mass, m_χ, of the lightest neutralino.

The observables we include in the likelihood are the same as in the previous section, listed in Table 2, for details see [10]. Also for this analysis, unlike the analysis done in the previous section, we impose (2σ) hard cuts, in all the available experimental constraints, on the resulting scan data. In Table 3 we give the range where our priors vary.

In Fig. 3 we display our results in the m_χ - σ_p^{SI} plane. We can see in the plot the regions

Parameter	Range	Parameter	Range
bino mass	$0.1 < M_1 < 30$	CP-odd neutral scalar Higgs mass	$85 < m_A < 600$
wino mass	$90 < M_2 < 500$	slepton-left mass	$70 < m_{\tilde{l}_L} < 3000$
μ parameter	$90 < \mu < 500$	slepton-right mass	$70 < m_{\tilde{l}_R} < 3000$
ratio of Higgs doublet s	$2 < \tan\beta < 65$	trilinear terms	$\lvert A_\kappa\rvert < 100$, $\lvert\tilde{A}\rvert < 4000$
Higgs sector coupling	$10^{-4} < \lambda < 0.5$	Higgs sector coupling	$10^{-4} < \kappa < 0.5$

Table 3. The prior ranges of input parameters over which we perform our scan of the NMSSM. All displayed mass ranges are given in GeV. We adopt log priors for all input parameters except $\tan\beta$, for which we use a flat prior.

favoured by DAMA/LIBRA [25] and CoGeNT [26] experiments. On the contrary, XENON-100 recent data seems to exclude this regions [27]. Likewise, the results from CDMS-II [28] seems to partially exclude the region favoured by CoGENT. At this point we want to recall that we are not including neither of this experiments in the likelihood function. We can clearly see that there are only a minority of our selected points that possess a significant singlino component that survive our cuts and generate a value of $\sigma_p^{SI} > 10^{-7}$ pb. The consequences of imposing the constraints from flavour physics are severe.

Finally, in Fig. 4 we present our results in the λ-κ plane with third axes displaying the singlet composition of the lightest Higgs scalar (left panel) and singlino composition of the lightest neutralino (right panel). We clearly observe that our scan points are segregated into several different regions in the λ-κ plane, each with a distinctive minimum value of $\log_{10}\lambda$, containing points that we can ascribe to one of approximately four different categories that we will now discuss.

Starting at small values of λ we observe the following categories of points: (i) At $\lambda \sim 10^{-4}$ we can see the onset of the MSSM-like region, consisting of bino-dominated LSPs with $m_\chi \gtrsim 7$ GeV, with the lightest Higgs scalar being doublet-like with $m_{h_1} \gtrsim 114.4$ GeV in order to evade LEP bounds. In this case the neutralino annihilates mainly through a t-channel slepton exchange. (ii) For $\lambda \sim 10^{-3}$ and $\kappa \sim 10^{-4}$ we observe the onset of a region where $m_\chi \gtrsim 15$ GeV and, as with the MSSM-like region, the LSP is bino-dominated and still annihilates mainly via t-channel slepton exchange, but in this case the lightest Higgs is singlet-like. (iii) For $\lambda \sim 10^{-2}$ we find the onset of those points involving bino-dominated neutralino LSPs that annihilate through a s-channel resonance involving a singlet-like Higgs, possessing a mass following the relation: $m_\chi \approx 2m_{h_1}$. iv) Lastly, for $\lambda \gtrsim 10^{-1}$ we find neutralinos with $m_\chi \lesssim 15$ GeV which are now a mixture of both singlino and bino and, as with (iii), annihilate via a resonance involving a singlet-like Higgs. A degree of fine-tunning is necessary in order to generate very light-singlet Higgses, pure enough to escape colliders constraints, far from the limit $\lambda \to 0$. Such solutions can potentially generate large values of the SI elastic scattering cross section that are several orders of magnitude larger than

that associated with the bino-dominated case, for $\lambda \sim 10^{-2}$, depending on the degree of fine-tuning involved. We must notice that we are using a log prior in λ and we are not taken into account dark matter direct detection experiments in the likelihood function. As a result, solution in the $\lambda \sim 10^{-2}$ region are much more frequently sampled than the extremely finely-tuned solutions in $\lambda \gtrsim 0.1$ and within the DAMA/LIBRA region. We can see that these extremely finely-tuned solutions are not surviving our (2σ) hard cuts, however such solutions have been found by several authors, see for example [30, 31].

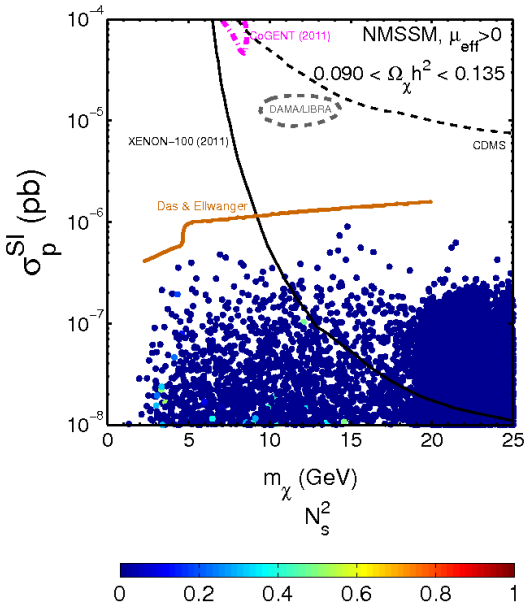

Figure 3. m_χ vs σ_p^{SI} in the NMSSM, for the points from our initial NS scan that survive subsequent 2σ hard cuts on $\Omega_\chi h^2$ and when using constraints from colliders (including flavour physics). The colour scale indicates the singlino fraction of each respective neutralino LSP. We also illustrate the regions of parameter space currently favoured by CoGENT (outlined by the magenta dash-dotted curve), DAMA/LIBRA (with ion channelling, outlined by the dashed grey curve), and illustrate the current limits from CDMS-II (dashed black curve) and XENON-100 (solid black curve). We also display the estimated upper bound on σ_p^{SI} in the NMSSM according to Das & Ellwanger [29] when using default values of strange quark content in nucleons (orange curve).

4. Summary

A global exploration of wide ranges of the CNMSSM parameters and a Bayesian analysis, show that from a statistical point of view, it is difficult to distinguish the model from the CMSSM, i.e., small values of λ are preferred (decoupled limit). As a result the neutralino dark matter direct detection cross section resembles the one obtained for the CMSSM.

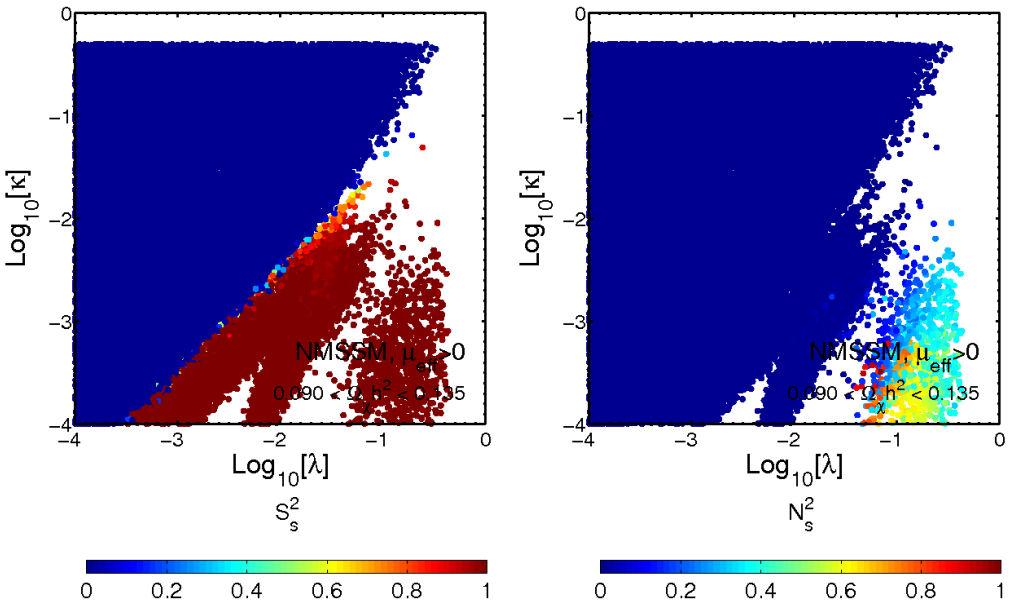

Figure 4. *Left panel:* $\log_{10}\lambda$ vs $\log_{10}\kappa$ in the NMSSM, for the points from our initial NS scan that survive subsequent 2σ hard cuts on $\Omega_\chi h^2$ and when using constraints from colliders (including flavour physics). The colour scale illustrates the singlet fraction S^2_S of the lightest Higgs. *Right panel:* Identical to the left panel except now the colour scale indicates the singlino fraction of each respective neutralino LSP.

In addition, using the power of the nested sampling (NS) algorithm, we investigate low mass neutralinos in the case of the NMSSM, making a scan of the low energy parameter space. For $m_\chi \lesssim 15$ GeV, we found a favoured region of Bino-dominated neutralinos, for $\lambda \sim 10^{-2}$, accessible to dark matter direct detection experiments. After invoking experimental constraints as 2σ hard cuts, particularly those coming from $BR(\overline{B}_s \to \mu^+\mu^-)$ and $\Omega_\chi h^2$, we find results very similar to those obtained in [29] where $\sigma_p^{SI} \lesssim 10^{-6}$ pb.

Acknowledgements

The work reported here was based in collaborations with D. T. Cumberbatch, J. F. Gunion, L. Roszkowski, R. Ruiz de Austri, Y-L S. Tsai and T. A. Varley. I gratefully acknowledge them. I wishes to thank the organizers of the DSU 2011, at Beijing, for their hospitality. This work was supported by the French ANR TAPDMS ANR-09-JCJC-0146, and in part by the Project of Knowledge Innovation Program (PKIP) of Chinese Academy of Sciences, Grant No. KJCX2.YW.W10.

References

[1] For a review see, U. Ellwanger, C. Hugonie and A. M. Teixeira, Phys. Rept. **496**, 1 (2010) [arXiv:0910.1785 [hep-ph]].

[2] D. G. Cerdeño, C. Hugonie, D. E. López-Fogliani, C. Muñoz and A. M. Teixeira, JHEP **0412** (2004) 048 [arXiv:hep-ph/0408102].
[3] D. G. Cerdeno, E. Gabrielli, D. E. Lopez-Fogliani, C. Munoz and A. M. Teixeira, JCAP **0706** (2007) 008 [arXiv: hep-ph/0701271]; D. E. Lopez-Fogliani, J. Phys. AA **40** (2007) 6889 [arXiv:hep-ph/0703181].
[4] J. Skilling, *Nested sampling*, AIP Conference Proceedings, 735 (2004), pp. 395–405.
[5] http://projects.hepforge.org/multinest/
[6] `http://superbayes.org/`
[7] U. Ellwanger and C. Hugonie, Comput. Phys. Commun. **177** (2007) 399 [arXiv:hep-ph/0612134]; http://www.th.u-psud.fr/NMHDECAY/nmssmtools.html
[8] D. E. Lopez-Fogliani, L. Roszkowski, R. R. de Austri and T. A. Varley, Phys. Rev. D **80** (2009) 095013 [arXiv:0906.4911 [hep-ph]].
[9] J. F. Gunion, D. E. Lopez-Fogliani, L. Roszkowski, R. Ruiz de Austri and T. A. Varley, Phys. Rev. D **84** (2011) 055026 [arXiv:1105.1195 [hep-ph]].
[10] D. T. Cumberbatch, D. E. Lopez-Fogliani, L. Roszkowski, R. R. de Austri and Y. -L. S. Tsai, arXiv:1107.1604 [astro-ph.CO].
[11] F. Feroz and M. P. Hobson, Mon. Not. Roy. Astron. Soc. **384** (2008) 449 [astro-ph/0704.3704].
[12] R. Trotta, F. Feroz, M. P. Hobson, L. Roszkowski and R. Ruiz de Austri, JHEP **0812** (2008) 024 [arXiv:hep-ph/0809.3792].
[13] L. Roszkowski, R. Ruiz de Austri, R. Trotta, Y.-L. S. Tsai, and T. A. Varley, Phys. Rev. D **83** (2011) 015014, [hep-ph/0903.1279].
[14] J. P. Miller, E. de Rafael and B. L. Roberts, Rept. Prog. Phys. **70** (2007) 795 [arXiv:hep-ph/0703049].
[15] The CDF Collaboration, Phys. Rev. Lett. **97** (2006) 062003 [hep-ex/0606027]; Phys. Rev. Lett. **97** (2006) 242003 [hep-ex/0609040].
[16] J. Dunkley et al. [The WMAP Collaboration], Astrophys. J. Suppl. **180** (2009) 306, arXiv:0803.0586 [astro-ph].
[17] The CDF Collaboration, *Search for $B_s \to \mu^+\mu^-$ and $B_d \to \mu^+\mu^-$ decays in $p\bar{p}$ collisions with CDF-II,* CDF note 8956 (August 2007).
[18] R. Ruiz de Austri, R. Trotta and L. Roszkowski, JHEP **0605** (2006)002 [arXiv:hep-ph/0602028]; see also R. Trotta, R. Ruiz de Austri and L. Roszkowski, New Astron. Rev. **51** (2007) 316 [astro-ph/0609126].
[19] The CDMS Collaboration, *Phys. Rev. Lett.* **96** (2006) 011302 [astro-ph/0509259].
[20] V. Sanglard *et al.*[EDELWEISS Collaboration], Phys. Rev. D **71** (2005) 122002 [astro-ph/0503265].
[21] G. J. Alner *et al.*[UK Dark Matter Collaboration], *Astropart. Phys.* **23** (2005)444.
[22] G. J. Alner *et al.*, Astropart. Phys. **28** (2007) 287 [astro-ph/0701858].
[23] V. N. Lebedenko *et al.*, Phys. Rev. D **80** (2009) 052010 arXiv:0812.1150 [astro-ph].
[24] J. Angle *et al.* [XENON Collaboration], Phys. Rev. Lett. **100** (2008) 021303 [astro-ph/0706.0039].
[25] R. Bernabei *et al.*, Eur. Phys. J. C **67** (2010) 39 [arXiv:1002.1028 [astro-ph.GA]].
[26] C. E. Aalseth *et al.* [CoGeNT collaboration], Phys. Rev. Lett. **106** (2011) 131301 [arXiv:1002.4703 [astro-ph.CO]]; C. E. Aalseth *et al.*, Phys. Rev. Lett. **107** (2011) 141301 [arXiv:1106.0650 [astro-ph.CO]].
[27] E. Aprile *et al.* [XENON100 Collaboration], Phys. Rev. Lett. **107** (2011) 131302 [arXiv:1104.2549 [astro-ph.CO]].
[28] Z. Ahmed *et al.* [The CDMS-II Collaboration], Science **327** (2010) 1619 [arXiv:0912.3592 [astro-ph.CO]].
[29] D. Das and U. Ellwanger, JHEP **1009** (2010) 085, [arXiv:1007.1151 [hep-ph]].
[30] G. Belanger, F. Boudjema, C. Hugonie, A. Pukhov and A. Semenov, JCAP **0509**, 001 (2005) [arXiv:hep-ph/0505142].
[31] http://higgs2.ucdavis.edu/gunion/blois_6_2_11.pdf